Non-impulsive source waveforms for physical modelling

Kevin W. Hall, Joe Wong, Kevin Bertram, and Kris Innanen

ABSTRACT

The physical modelling system is being upgraded with an arbitrary waveform generator (AWG), that will allow us to use non-impulsive source waveforms including sinusoidal frequency sweeps, square-wave frequency sweeps, and m-sequences (pseudorandom binary sequences). Some of these waveforms, such as constant amplitude mono-frequency square waves or mono-frequency spike series can be run without an AWG. Square wave signals and spike series have only two normalized values: +1 and -1. Therefore, they are called binary-valued sequences, and are much more easily generated by electronic circuits for practical usage than are sinusoidal signals.

This report examines the theoretical effect of running a variety of source waveforms, including Vibroseis sweeps, through our system, and predicts our future results if we use a pair of millimeter-sized source transducers, which have a characteristic impulse response. We also show actual data resulting from a spike series run through 37 mm buzzers. Of interest for all source waveforms is the expected amplitude at the receiver for 10 kHz (equivalent to 1 Hz after scaling by 10000 to real-world seismic exploration frequencies), which we need if we wish to run full-waveform inversions (FWI) on physically modeled data. Our results show that running a frequency sweep that spends proportionately more time near 1 Hz (scaled) can improve our recorded amplitudes at that frequency, but enhancing this signal will require further processing.

INTRODUCTION

Spread spectrum techniques are a way to obtain a good estimate of the impulse response of a linear system in high-noise situations. If one were to use an impulse to generate a detectable signal, the energy and peak power of the impulse might need to be dangerously high in order to overcome the noise. However, if we spread the required energy over a long period of time, the power of the source signal can be reduced to safe levels while the total energy remains high. The problem then becomes one of compressing the distributed energy back to an impulse-like signal. This is called synthetic pulse acquisition. Two types of distributed-energy signals have been found to be highly amenable for easy pulse compression: frequency sweeps and pseudo-random periodic signals.

For inversions, including full waveform inversions, we desire low frequencies in our seismic data. Typically, we would like to have significant energy at least as low as one Hz for seismic data (equivalent to 10 kHz for the physical modelling system. Figures in this report will be scaled to seismic frequencies, as that makes it easier to compare to seismic data. We are building an arbitrary waveform generator and amplifiers (Wong et al., 2020) that will allow us to run Vibroseis sweeps and pseudo-random periodic signals through our piezoelectric transducers. The questions that we wish to at least partially answer in this report are: 1) what will Vibroseis sweep data look like once we can run sweeps on our physical modelling system, 2) can we compensate for issues with low-

amplitudes at certain frequencies by modifying those sweeps, and 3) can we generate our target frequency content using other methods, such as pulsing the piezo-electric transducers (spike series) or by using maximal length sequences (m-sequences).

METHOD

It is easier to generate constant amplitude square waves or spike series in our electronics than it is to generate sinusoids with varying amplitudes. For example, we can create the former using a single GPIO pin on a Raspberry Pi but require 9 GPIO pins to create a sinusoid. Given a Vibroseis sweep harvested from the auxiliary traces of an uncorrelated shot gather, we can convert the sweep to a square wave sweep by considering just the sign of each sample (plus one or minus one). The square wave sweep can be further converted to a spike series by taking the sample-to-sample difference of the square wave. These signals can be digitized and stored as 16-bit integers in a file. In the physical-modelling laboratory, the file is read by a Raspberry Pi 4B microcomputer and the data are sent out as a bit stream to an R2R resistor ladder that effectively converts the digitized data to an analogue signal. The analogue signal is amplified to a high voltage to drive piezoelectric transducers. Comparison of resulting amplitude spectra will then help us to determine the relative merits of each input signal for a given frequency or frequency band.

Figure 1 shows the two types of transducers that are considered in this report, 37 mm buzzers (a) and piezo-pins (b). Our usual scale factor for the physical modelling system is 1:10000. This means that a 1 mm piezo-pin placed on a physical model scales to 10 m in the real world. Similarly, a 37 mm buzzer scales to 370 m. Clearly, we would prefer to use the smallest transducer we can get away with, but we predict that we will be able to generate lower frequencies with a larger transducer.

Piezo-pin impulse response

Figure 2a shows the impulse response for a single spike input signal to a piezo-pin transducer, recorded on an identical transducer at zero offset. The amplitude spectrum (Figure 2b) is plotted below a vertical red line at 1 Hz (our frequency of interest) and a horizontal magenta line at 30 dB down. The magenta line represents our rule of thumb for seismic data, where we will be unable to see any amplitudes less than 30 dB down when the data are plotted without further processing/scaling. The red and magenta lines will be shown on all amplitude spectra plots in this report. This amplitude spectrum for unprocessed data shows good amplitudes between about 25 and about 60 Hz with a couple of notches within this narrow frequency range. Amplitudes at 1 Hz for all figures in this report are listed in Table A1.

Land seismic sweeps

Figures 3 and 4 show linear and low-dwell 1-100 Hz sweeps from the Hussar low-frequency experiment (Isaac and Margrave, 2011). For this and similar figures in this report, the figure shows: The source waveform (a), the first 20 Hz of the amplitude spectrum of the source waveform (b), the autocorrelation of the source waveform (c), the sign of the source waveform (d), the first 20 Hz of the amplitude spectrum of the sign of

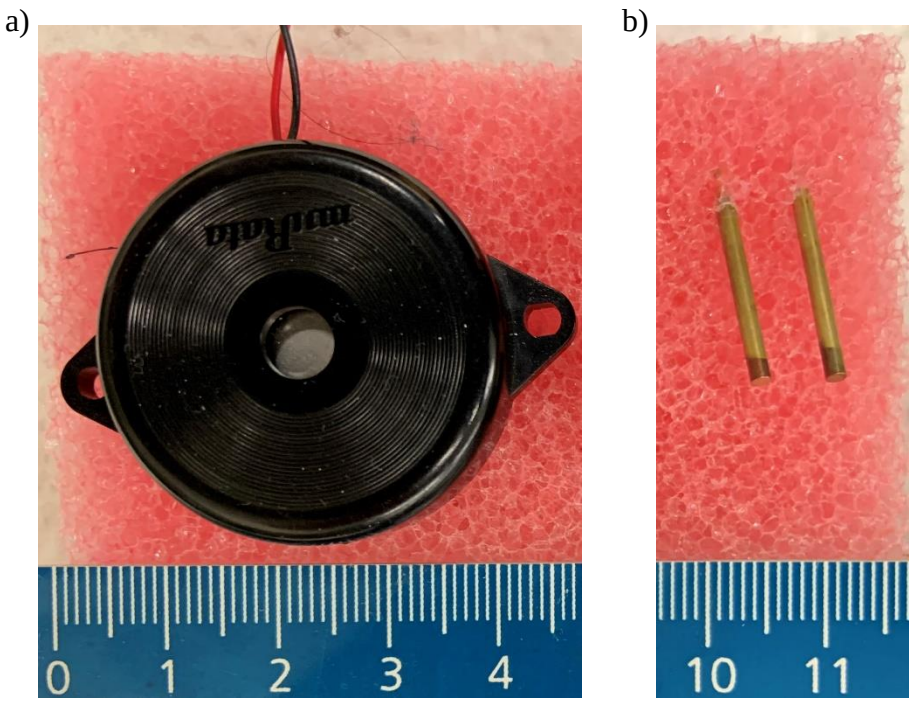

FIG. 1. (a) 37 mm Buzzer, and (b) piezo-pins.

RESULTS

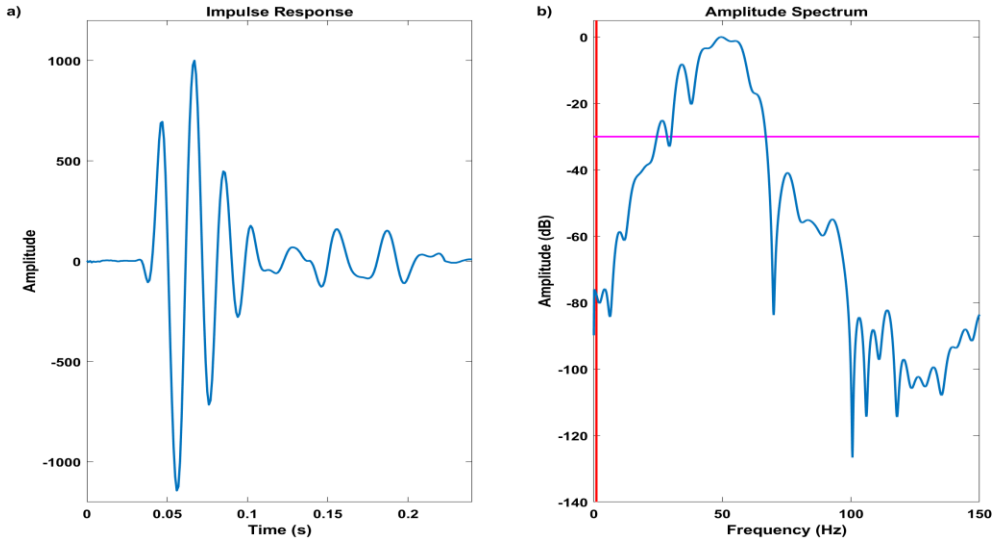

FIG. 2. Impulse response (a) and amplitude spectrum (b) for a pair of piezo-pin transducers (Figure 1b).

the source waveform (e), the autocorrelation of the sign of the source waveform, (f) the result of convolving the sign of the source waveform with the piezo-pin impulse response (g), the first 20 Hz of the amplitude spectrum of the sign of the source waveform convolved with the impulse response (h), and the autocorrelation of the sign of the source waveform convolved with the impulse response. The bottom row of these figure, then, is our prediction of what the data will look like once we are able to run this frequency sweep on the physical modelling system if we use the piezo-pin transducers. Like Figure 2, a vertical red line is plotted at 1 Hz a horizontal magenta line is plotted at 30 dB down, and the amplitude at 1 Hz is listed in Table A1.

Conversion to a square wave does more damage to the low-dwell sweep wavelet than to the linear sweep wavelet (compare Figure 3e and 3f to 4e and 4f). However, convolution with the piezo-pin impulse response results in an almost identical wavelet (Figures 3i and 4i), which has larger side-lobes than we see for the unaltered sweep (Figures 3c and 4c). The low-dwell sweep has higher amplitudes at 1 Hz than the linear sweep after convolution with the impulse response (Figures 3h and 4h). As expected, this implies that we should be able to increase recorded amplitudes at 1 Hz if we spend longer at that frequency during the sweep.

Mono-frequency sweeps

In the absence of an arbitrary waveform generator, we can attempt to improve our 1 Hz piezo-electric transducer response by using a 1 Hz mono-frequency sweep, or sine wave converted to a square wave (Figure 5a) or spike-series with positive spikes only (Figure 6a), or a spike series with positive and negative spikes (Figure 7a). While the amplitude spectrum for the input sine wave looks quite good, with a well-defined spike at 1 Hz (Figure 5b, 6b, and 7b), conversion to a square waves or spike series (Figure 5d, 6d, and 7d) results in periodic spikes in the amplitude spectra (Figure 5e, 6e, and 7e), which is diagnostic of aliasing. Convolution with the impulse response also shows periodic spikes in the amplitude spectrum, as we would expect. The resulting wavelet has an unexpected low frequency component, together with multiple copies of the wavelet due to aliasing (Figures 5i, 6i and 7i), although this is most obvious in the square wave data (Figure 5i). However, we do have very good amplitudes at 1 Hz. These data could potentially be filtered with a narrow bandpass filter to remove the aliased signal and retain just the narrow-band 1 Hz data that we are interested in while discarding all other frequencies in the data that are brought in by the impulse response (cf. Figure 2).

Narrow bandwidth sweeps

If we have an arbitrary waveform generator, we can mitigate the aliasing observed in our mono-frequency sweep by switching to a narrow-bandwidth sweep. Figure 8a shows the results for a long 0.5 to 1.5 Hz sweep. The amplitude spectrum for this sweep shows no signs of aliasing, but, convolution with the piezo-pin impulse response knocks our 1 Hz amplitude down to- 93 dB, as compared to -88 dB down for broad-band Vibroseis sweep shown in Figure 4.

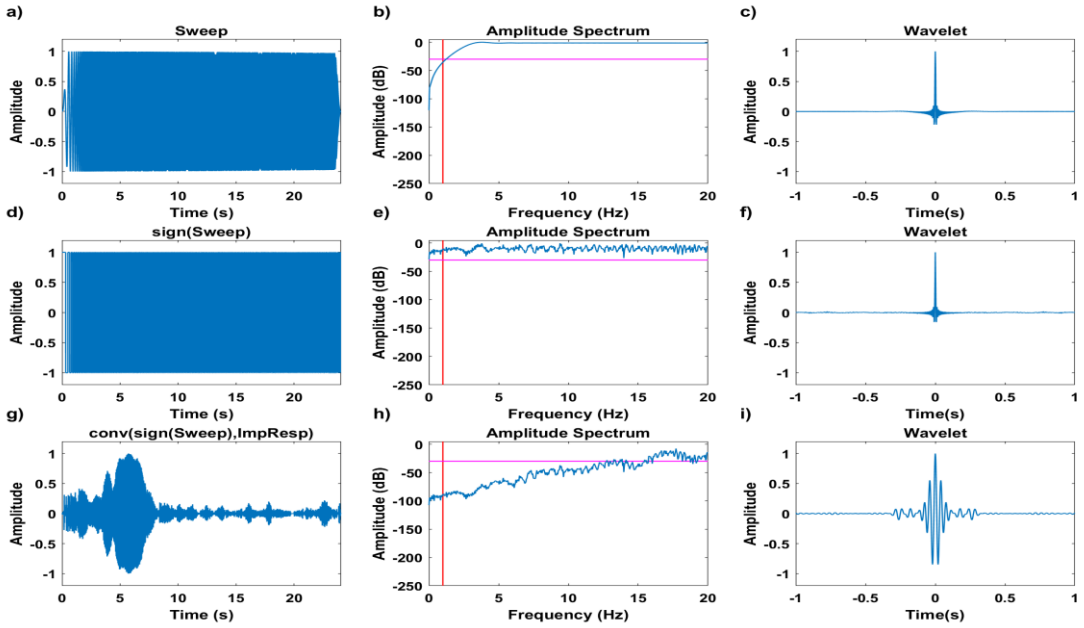

FIG. 3. Top row: (a) Linear 1-100 Hz, 24 s sweep from the Hussar 2011 low-frequency experiment (Inova Vibe), (b) amplitude spectrum of 3a and, (c) wavelet after autocorrelation of 3a. Middle row: (d) 3a converted to a square wave, (e) amplitude spectra of 3d, and (f) wavelet after autocorrelation of 3d. Bottom row: (g) convolution of 3d with piezo-pin impulse response, (h) amplitude spectra of 3g, and (i) wavelet after autocorrelation of 3g.

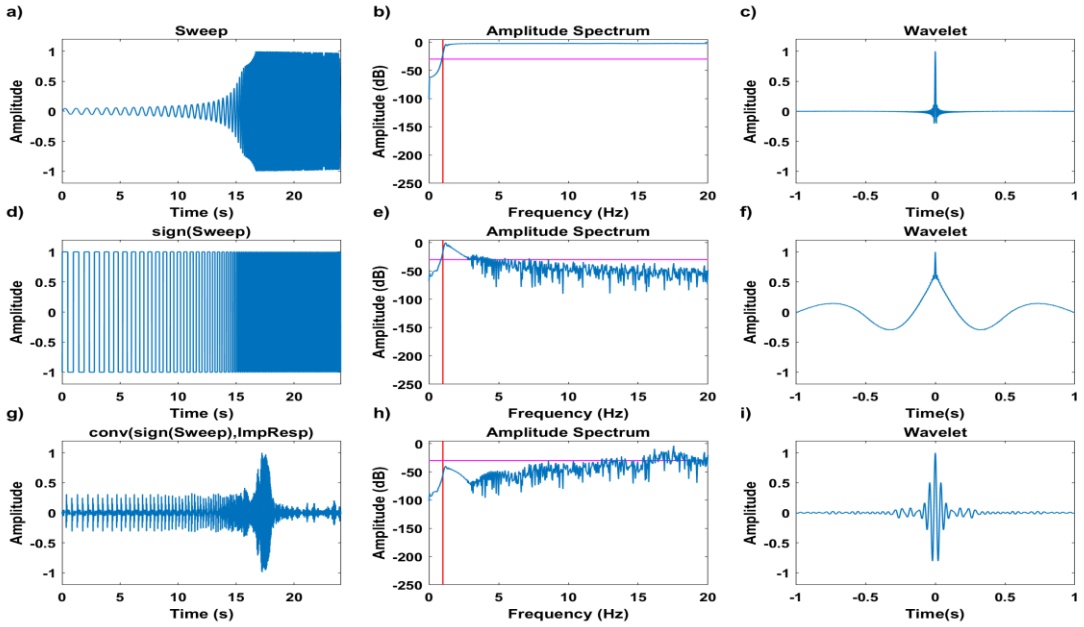

FIG. 4. Top row: (a) Low-dwell 1-100 Hz, 24 s sweep from Hussar 2011 low-frequency experiment (Failing Vibe), (b) amplitude spectrum of 4a and, (c) autocorrelation of 4a. Middle row: (d) 4a converted to a square wave, (e) amplitude spectra of 4d, and (f) autocorrelation of 4d. Bottom row: (g) convolution of 4d with piezo-pin impulse response, (h) amplitude spectra of 4g, and (i) wavelet after autocorrelation of 4g.

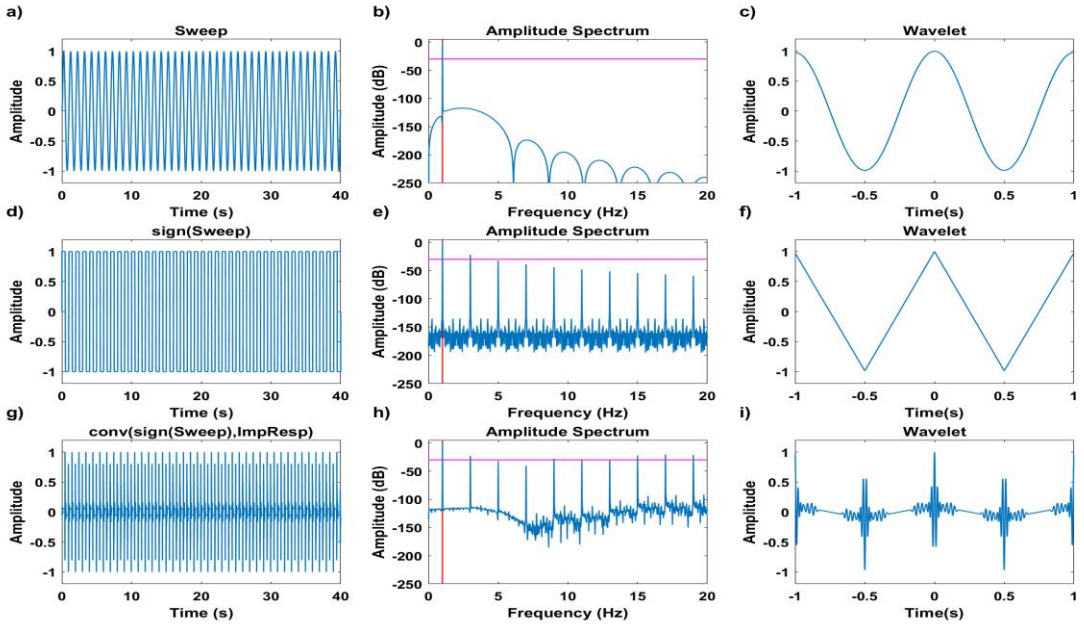

FIG. 5. Top row: (a) 1 Hz, 40 s mono-frequency sweep, (b) amplitude spectrum of 5a and, (c) autocorrelation of 5a. Middle row: (d) 5a converted to a square wave, (e) amplitude spectra of 5d, and (f) autocorrelation of 5d. Bottom row: (g) convolution of 5d with piezo-pin impulse response, (h) amplitude spectra of 5g, and (i) wavelet after autocorrelation of 5g.

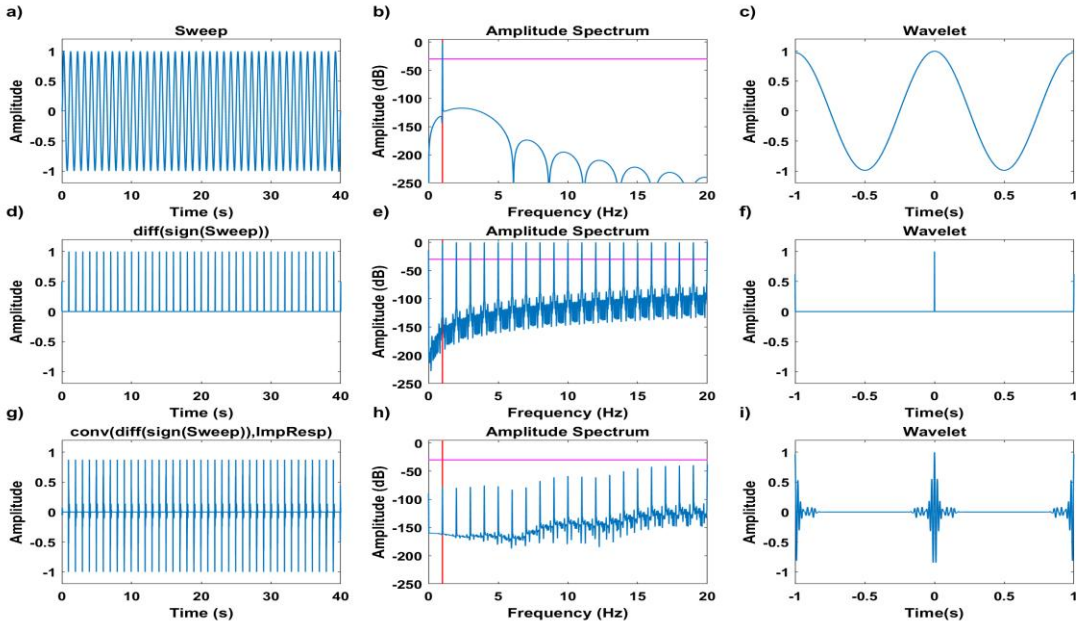

FIG. 6. Top row: (a) 1 Hz, 40 s mono-frequency sweep (b) amplitude spectrum of 6a and, (c) autocorrelation of 6a. Middle row: (d) 6a converted to a spike series with negative amplitudes removed, (e) amplitude spectra of 6d, and (f) autocorrelation of 6d. Bottom row: (g) convolution of 6d with piezo-pin impulse response, (h) amplitude spectra of 6g, and (i) wavelet after autocorrelation of 6g.

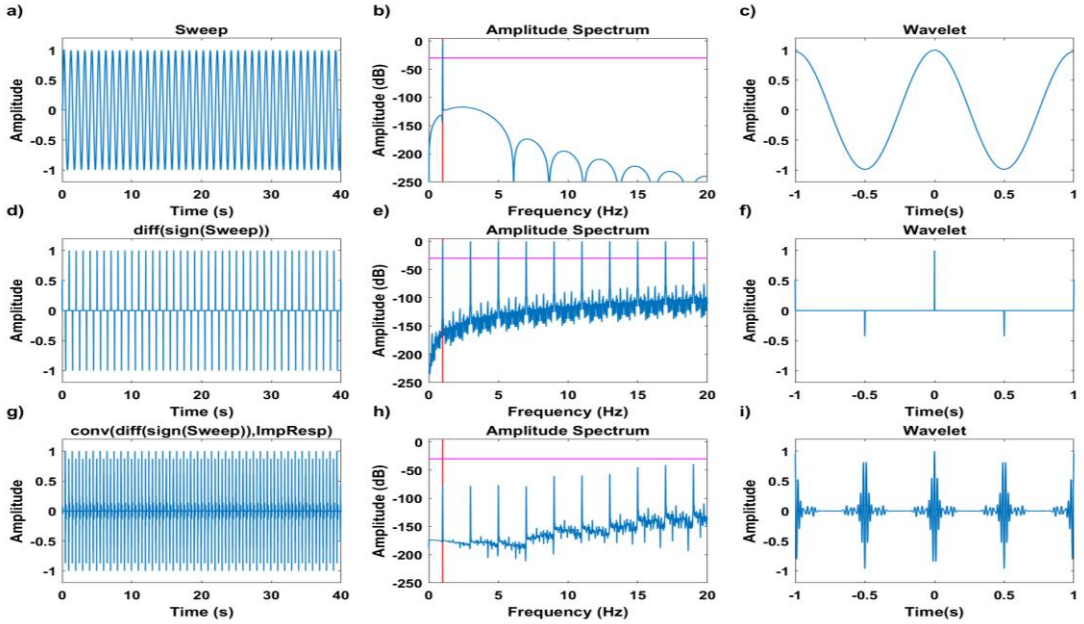

FIG. 7. Top row: (a) 1 Hz, 40 s mono-frequency sweep, (b) amplitude spectrum of 7a and, (c) autocorrelation of 7a. Middle row: (d) 7a converted to a spike series, (e) amplitude spectra of 7d, and (f) autocorrelation of 7d. Bottom row: (g) convolution of 7d with piezo-pin impulse response, (h) amplitude spectra of 7g, and (i) wavelet after autocorrelation of 7g.

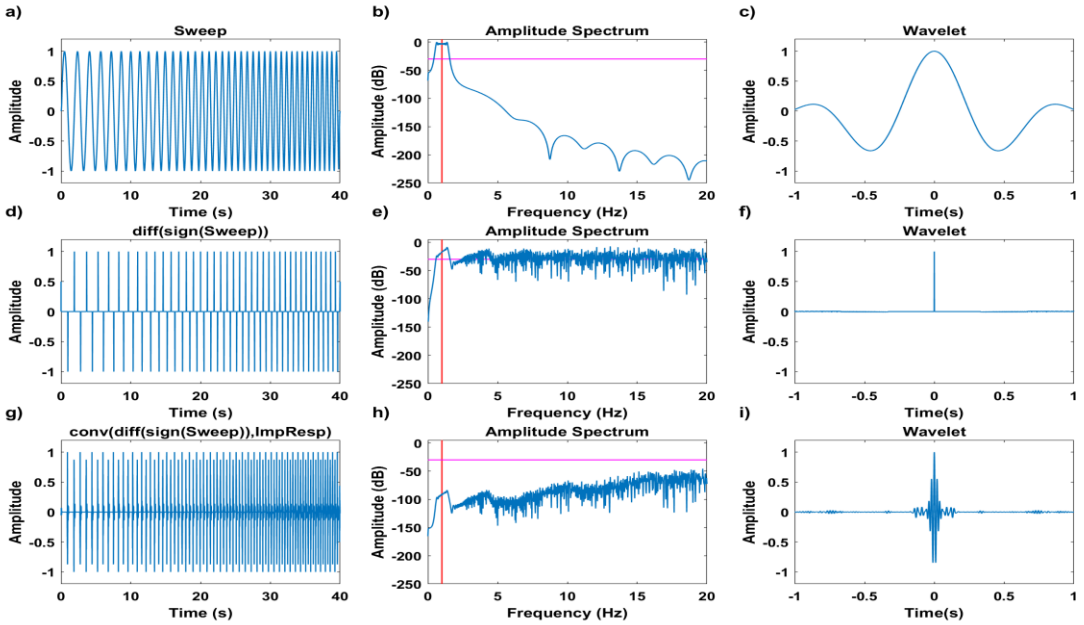

FIG. 8. Top row: (a) 0.5-1.5 Hz, 40 s sweep, (b) amplitude spectrum of 8a and, (c) autocorrelation of 8a. Middle row: (d) 8a converted to a spike series, (e) amplitude spectra of 8d, and (f) autocorrelation of 8d. Bottom row: (g) convolution of 8d with piezo-pin impulse response, (h) amplitude spectra of 8g, and (i) wavelet after autocorrelation of 8g.

Maximal length sequences

Maximal-length sequences (or m-sequences) are a type of pseudo-random binary sequence (PRBS). They are well-defined mathematical constructs intimately connected with so-called primitive or irreducible polynomials (Watson, 1962). In practice, m-sequences are easily produced by logic statements in software. They also can be generated electronically by simple circuits known as linear shift registers (Golomb, 1967; Golomb and Gong, 2005; Holmes, 2007).

A m-sequence (Figure 9) is a periodic stream of 1's and -1's characterized by its degree m, its fundamental length L, and its base period t_b. The sequence fundamental length L isgiven by:

$$L = 2^m - 1 \, . \tag{1}$$

The base period t_b is the shortest time in the sequence between transitions from one binary value to the other. The m-sequence is periodic, and repeats itself after a time

$$T_m = L \cdot t_b \, . \tag{2}$$

For seismic applications, it is convenient to express T_m in milliseconds. For digitized versions, we also specify the sample time t_s, with

$$t_s = t_b / r \, , \tag{2}$$

where r is an integer (typically equal to 1, 2, 4, 8, or 16) that determines over-sampling of the m-sequence. The over-sampled length is equal to rL points.

The autocorrelation of a sampled m-sequence is also periodic, showing a series of triangular peaks with peak value equal to rL and off-peak values equal to $-r$. If we remove the factor r, we obtain scaled peak and off-peak values of L and -1, respectively. These autocorrelation values are fundamental properties of any m-sequence. The widths of the triangles extend from $-r$ samples to $+r$ samples symmetrically about the peaks.

The normalized amplitude spectrum of an m-sequence approximates the normalized amplitude spectrum of a square impulse with duration time equal to the base period (the amplitude spectrum of a square impulse is a sinc function). The longer the time length of the sequence, the better the approximation will be (Figure 10). Note that the first notch in the spectrum occurs at a frequency equal to $1/t_b$. There is much literature on using m-sequences for data acquisition in engineering and earth science has been reported (see the reference list).

Figure 11 shows our predicted result for an example m-sequence. Once again, our amplitude a 1 Hz is harmed by convolution with the piezo-pin impulse response, but the side-lobes of the resulting wavelet are noticeably smaller than predicted for Vibroseis sweeps (compare with Figures 3 and 4).

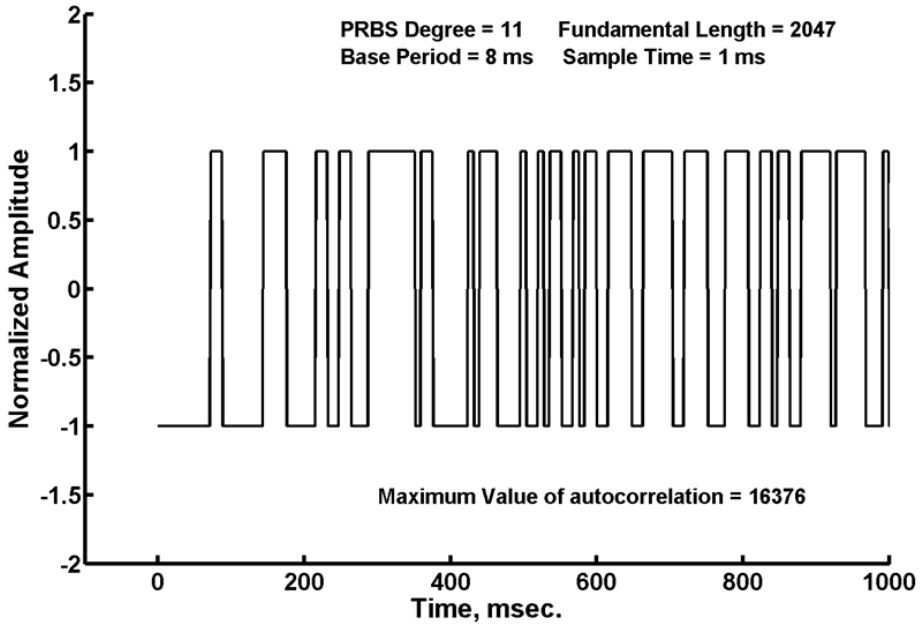

FIG. 9. First 1000 ms of an example m-sequence for driving vibratory sources: m-sequence degree = 11; m-sequence fundamental length = 2047; base period = 8 ms; sample time = 1 ms; number of digital points = 16376; time length of m-sequence = 16376 ms.

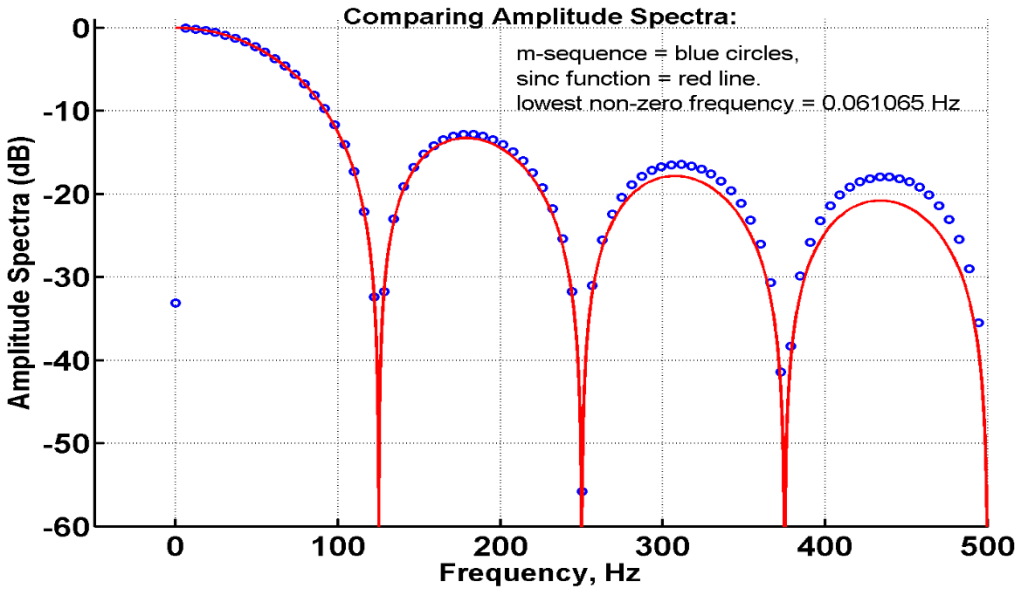

FIG. 10. Amplitude spectrum of the example m-sequence compared to the amplitude spectrum of the sinc function defined by $\mathrm{sinc}(i) = \mathrm{abs}(\sin(\omega(i)*t_b/2)/\omega(i))$, where $\omega(i)$ is the radian frequency, and t_b is the m-sequence base period in seconds.

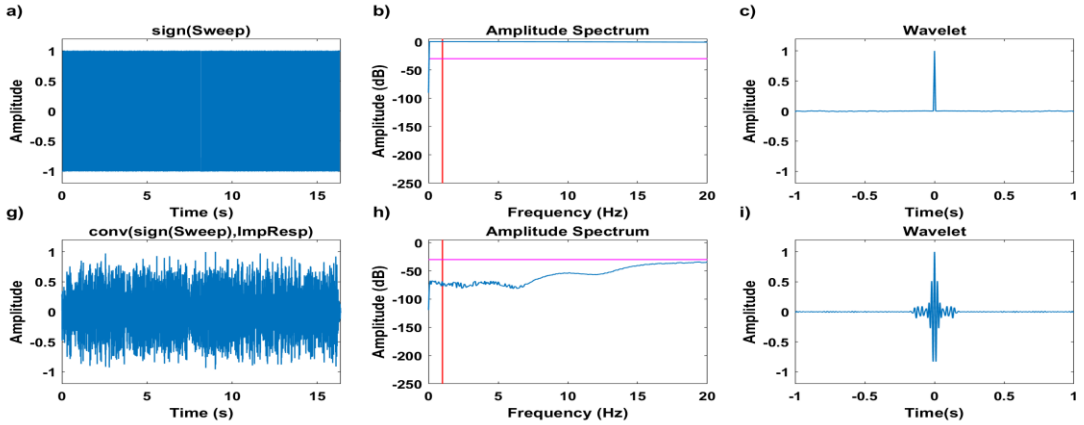

FIG. 11. Top row: (a) M-sequence, (b) amplitude spectrum of 11a and, (c) wavelet after cross-correlation of 11a. Middle row: Not shown, because taking the sign of an m-sequence gives a result that is identical to the input. Bottom row: (g) convolution of 11a with piezo-pin impulse response, (h) amplitude spectra of 11g, and (i) wavelet after autocorrelation of 11g.

Buzzer data

Figure 12 shows actual results from the physical modelling system for 37 mm buzzers at zero-offset in water before water seepage altered the response (top) and for the same buzzers in the air after water seepage altered the response (bottom) for a 10 kHz (1 Hz scaled) spike series with positive spikes only. These data are most like the theoretical results shown in Figure 6. Amplitudes near zero and periodic spikes in the amplitude spectra, which are more obvious in the amplitude spectra if we do not constrain ourselves to the first 20 Hz (not shown), and the ringy character of the data are almost certainly due to aliasing.

Figure 13 shows a walk-away survey acquired with 37 mm buzzers immersed in water, with traces acquired as the buzzers are progressively moved away from each other. Using a scale factor of 10000, the modelled trace spacing is 10 m. There is significant near-zero Hz energy in this data, which have had the mean subtracted and a linear trend removed before plotting. The dipping red line (Figure 13a) was calculated using a water velocity of 1485 m/s and arbitrarily plotted beginning at 0.5 s for comparison with the signal. This shows that we can make valid velocity measurements using aliased data acquired using the 37 mm buzzers.

DISCUSSION AND FUTURE WORK

Regardless of the input source waveform, our ability to record 1 Hz (scaled) data from piezo-pin transducers is primarily constrained by the impulse response of the piezo-pin. We need to compensate for this by spending proportionally more of the sweep time at 1 Hz (low-dwell non-linear sweeps), or possibly consider the use of larger diameter transducers.

Without access to an arbitrary waveform generator, we can run mono-frequency square waves and spike series. However, this results in heavily aliased data. If we are only interested in 1 Hz (for example), it may be possible to isolate this frequency with a

very narrow bandpass filter. We can measure the velocity of sound in some medium such as water with aliased data, but it would be better to record unaliased data.

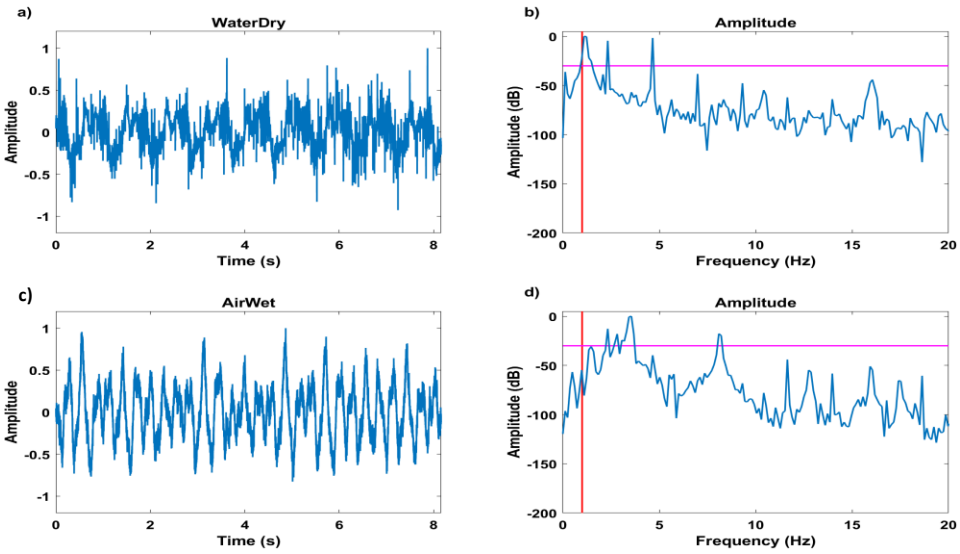

FIG. 12: Top row: (a) Buzzer data for 37 mm dry buzzers in water before water seepage changes the response and, (b) the amplitude spectrum for 12a. Bottom row: (c) Buzzer data for 37 mm wet buzzers in the air before they dry out enough to change the response and (d) the amplitude spectrum for 12c

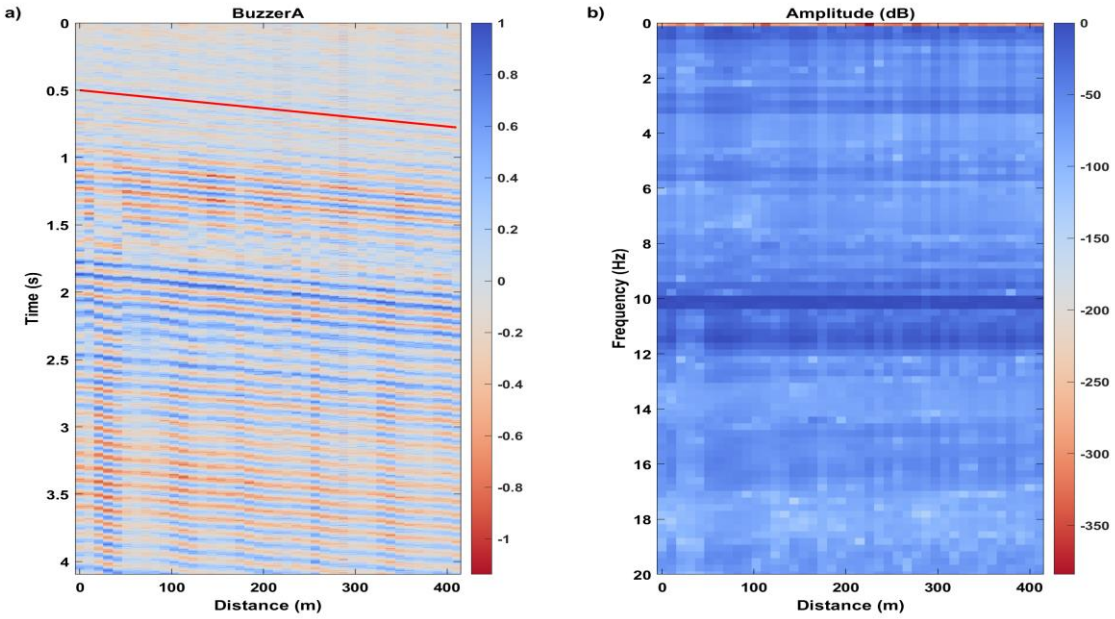

FIG. 13. Walk-away data for 37 mm buzzers in water after subtracting the mean and applying a linear detrend to each trace. No filters or AGC. The red reference line plotted over top of 13a was calculated using 1485 m/s (water velocity) and arbitrarily positioned to begin at 0.5 s.

Standard Vibroseis sweeps are severely harmed by convolution with the piezo-pin impulse response, which results in large side-lobes in the wavelet that results from cross-correlation. M-sequence source waveforms are less affected and have noticeably smaller side-lobes than the Vibroseis sweeps after cross-correlation. However, while unmodified m-sequences have good amplitudes at 1 Hz, convolution with the impulse response still reduces those amplitudes significantly.

Real measurements in the Physical Modelling Laboratory must use a real transducer driven by a real electronic signal. The values on Table A1 in the Appendix clearly indicate that the best combination to use if we want get significant energy at 1 Hz (scaled) is that of the 37-mm-diameter buzzer driven by the m-sequence, or that of the piezo-pin driven by the Failing low-dwell sweep. The 37-mm buzzer is too large to be ideal for physical modelling, so we will test smaller 13-mm-diameter buzzers to determine their amplitude response at 1 Hz (scaled) compared to the amplitude at 50 Hz (50 Hz is an important parameter because real seismograms from the exploration world generally exhibit reflection wavelets with dominant frequencies near 50 Hz).

Once the arbitrary waveform generator is functional, we will be able to run Vibroseis sweeps and m-sequences through a variety of transducers and compare with our predicted results. It may be possible to design non-linear sweeps to compensate for the physical characteristics of the piezoelectric transducers. These will likely be much longer than sweeps that are typically used for land seismic. It would also be worth investigating post-acquisition frequency compensating processing steps such as spectral whitening or Gabor deconvolution.

ACKNOWLEDGEMENTS

We thank the sponsors of CREWES for continued support. This work was funded by CREWES industrial sponsors, NSERC (Natural Science and Engineering Research Council of Canada) through the grant CRDPJ 461179-13, and in part by the Canada First Research Excellence Fund.

REFERENCES

Behringer, D., Birdsall, T., Brown, M., Cornuelle, B., Heinmiller, R., Knox, R., Metzger, K., Munk, W., Speisberger, J., Spindel, R., Webb, D., Worcester, P., Wunsch, C., 1982, A demonstration of ocean acoustic tomography: Nature, 299, 121-125.

Duncan, P.M., Hwang, A., Edwards, R.N., Bailey, R.C., and G.D. Garland, 1980. The development and applications of a wide band electromagnetic sounding system using a pseudo-noise source: Geophysics, **45**, 1276-1296.

Dushaw, B.D., Howe, B.M., Mercer, J.A., and Spindel, R.C., 1999, Multi-megameter-range acoustic data obtained by bottom mounted hydrophone arrays for measurement of ocean temperature: IEEE J. of Ocean Engineering, **24**, 202-214.

Engelberger, S., and Benjamin, H., 2005, Pseudo-random sequences and the measurement of the frequency response: IEEE Instrumentation and Measurement Magazine, **8**, 54-59.

Golomb, S., 1967, Shift register sequences: Holden-Day, San Francisco.

Golomb, S.W., and Gong, G., 2005. Signal design for good correlation: for wireless communication, cryptography, and radar: ISBN-0-521-82104-5.

Holmes, J.K., 2007. Spread spectrum systems for GNSS and Wireless Communications, Artech House, Norwood, ISBN-9787-59693-083-4.

Isaac, J. H., and Margrave, G. F., 2011, Hurrah for Hussar! Comparisons of stacked data: *CREWES Research Report*, **23**, 55.1–55.23.

Watson, E.J., 1962. Primitive Polynomials (Mod 2): Math. Comp., **16**, 368-388.

Wong, Joe, 2012. Spread spectrum techniques for seismic data acquisition, CREWES Research Reports, **24**, 82.1-82.20.

Wong, J., Bertram, K., Zhang, H., Hall, K., and Innanen, K., 2020, Enhanced source hardware and tank for physical modelling: *CREWES Research Report*, This Volume.

Wong, J., Hurley, P., and West, G.F., 1983, Cross-hole seismic scanning and tomography: The Leading Edge, **6**, 31-34.

Ziolkowski, A., Wright, D, and Mattson, J., 2011. Comparison of PRBS and square-wave transient EM over Peon Gas Discovery, Norway, SEG Exp. Abstracts, **30**, 583-588.

APPENDIX A

Table A1 lists the amplitude at 1 Hz for a variety of real and synthetic datasets. If the data is shown in this report, the table includes the figure number. If the signal is aliased, the Aliased column has a 'Y.' If the source waveform requires an arbitrary waveform generator, the AWG column has a 'Y.'

Table A1. Amplitudes at 1 Hz

Figure	A (dB)	Aliased	AWG	Filename
2	-77.6			piezoPin_wavelet
	-55.3		Y	Hussar_Failing_Low_Dwell_1-100Hz_24s_0.2cosTapers.sgy
3h	-88.3		Y	Hussar_Inova_Linear_1-100Hz_24s_0.5cosTapers.sgy
4h	-76.7		Y	Hussar_Inova_Low_Dwell_1-100Hz_24s_0.2cosTapers.sgy
	-138.7		Y	Pretzel_IVI_Linear_10-150Hz_16s_0.2cosTapers.sgy
	-93.6		Y	Snowflake_Inova_Linear_1-150Hz_16s_0.2cosTapers.sgy
	-139.1		Y	VermillianLakes_Inova_Linear_10-100Hz_10s_0.2cosTapers.sgy
	-0.1	Y		4 cycles at 1 Hz square wave
	-77.7	Y		4 cycles at 1 Hz plus spikes
	-77.3	Y		4 cycles at 1 Hz plus/minus spikes
5h	-0.1	Y		40 cycles at 1 Hz square wave
6h	-77.3	Y		40 cycles at 1 Hz plus spikes
7h	-77.2	Y		40 cycles at 1 Hz plus/minus spikes
	-96.6		Y	40 cycles 0.5-1.5 Hz plus spikes
8h	-93.2		Y	40 cycles 0.5-1.5 1 Hz plus/minus spikes
12	-71.6		Y	mSeq_deg11_BP(ms)8
13b	-19.4	Y		bzzrWaterDry
13d	-58.8	Y		bzzrAirWet
13	-57.6	Y		buzzerA